Hysteresis-Free Lead-Free Double Perovskite Solar Cells by Interface Engineering

Martina Pantaler [1,2,†], Kyung Taek Cho [1,†], Valentin I. E. Queloz [1], Inés GarcíaBenito[1], Christian Fettkenhauer[2], Irina Anusca[2] , Mohammad Khaja Nazeeruddin [1,*], Doru C. Lupascu [2,*], Giulia Grancini [1,*]

[1] Group for Molecular Engineering of Functional Materials, Institute of Chemical Sciences and Engineering, Ecole Polytechnique Fédérale de Lausanne, Sion CH-1951, Switzerland.

[2] Institute for Materials Science and Center for Nanointegration Duisburg-Essen (CENIDE), University of Duisburg-Essen, Universitätsstraße 15, 45141 Essen

Corresponding Author

*Giulia.grancini@epfl.ch; doru.lupascu@uni-due.de; mdkhaja.nazeeruddin@epfl.ch

ABSTRACT. Hybrid perovskite solar cells have been creating a big excitement in the photovoltaic community. However, they still rely on toxic elements imposing severe limits for their commercialization. Lead-free double hybrid perovskites in the form of $Cs_2AgBiBr_6$ have been shown as a promising non-toxic and highly stable alternative. Nevertheless, device development is still at its infancy and performances affected by severe hysteresis. Here we realize for the first time hysteresis-free mesoporous double perovskite solar cells with no *s*-shape in the device characteristic and increased device open circuit voltage. This has been realized by fine tuning the material deposition parameters, enabling the growth of a highly uniform and compact $Cs_2AgBiBr_6$, and by engineering the device interfaces, upon screening different molecular and polymeric hole transporting materials (HTM). Our work represents a crucial step forward in lead-free double perovskite with significant potential for closing the gap for their market uptake.

TOC GRAPHICS
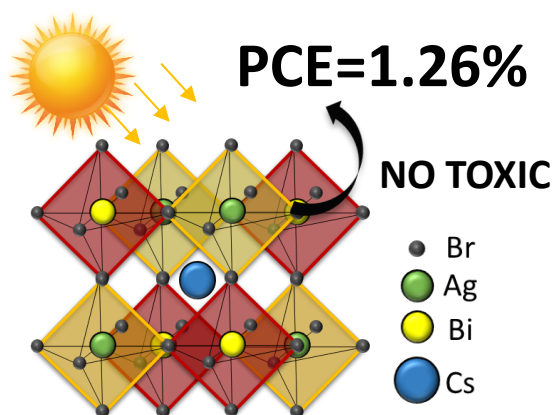
Since their advent, organic-inorganic hybrid perovskite solar cells (PSC) unleashed a great deal of enthusiasm in the photovoltaic (PV) research community. With power conversion efficiency (PCE) surpassing 22% upon only 9 years of research[1,2], this technology has a full potential to stand out over the PV solutions, such as dye sensitized solar cells, organic polymer solar cells, and even commercial polycrystalline Si solar cells, leaders of current market.[1,2] However, despite their excellent performances resulting in their high efficiency, they suffer from a poor device stability issue, mainly due to perovskite material degradation upon moisture and light exposure.[3,4,5,6] In addition, they rely on toxic lead, representing a serious drawback for PSC commercialization, with the associated health and environment concerns.[7,8] Huge theoretical effort in screening "less toxic" materials is ongoing. Tin (Sn) has first been used by replacing the position of Pb^{2+} as $MASn_xPb_{1-x}I_3$ now reaching PCE of 12%.[9] However, easily prone to oxidation (Sn^{2+} into Sn^{4+}) or incorporated in A_2SnX_6 structures (e.g. Cs_2SnI_6),[10,11] which exhibit better stability due to the presence of Sn in its stable oxidation state, the efficiency decayed rapidly in ambient condition.[12,13,14] To solve this problem, "quasi-2D perovskites" in the form of $(PEA)_2(FA)_{n-1}Sn_nI_{3n+1}$ were also suggested as a possible solution to improve material stability.[15] They have been obtained by mixing the different organic cations in a sort of bulk heterojunction structure, where the PEA molecules infiltrate at the boundary of perovskite grains blocking the oxygen diffusion into the perovskite lattice.[15] This resulted into a PCE up to 6% at enhanced stability. Other quasi 2D perovskites in the form of $(BA)_2(MA)_{n-1}Sn_nI_{3n+1}$ have also been developed showing promising PCE of around 2.5% for $n = 4$, stable for more than 1 month.[16] However, despite the improvements, the presence of Sn cannot be entirely out of the concerns about toxicity as to organism environment.[8] Instead of considering other divalent cations to eliminate the toxic Pb^{2+}, recent works have demonstrated the substitution of the two divalent Pb^{2+} ions into one monovalent ion M^+ and another trivalent ion M'^{3+}, while

keeping the total number of valence electrons unchanged at the halogen sites. The structure reads as $A_2M'^{1+}M'^{3+}X_6$, where A=Rb^+, Cs^+, $CH_3NH_3^+$, M^+=Na^+, K^+, M'^{3+}= Bi^{3+}, and X^-=Cl^-, Br^-, reported since back to the 1970s[17,18,19,20,21]. Among these, experimental synthesis of $Cs_2AgBiCl_6$ and $Cs_2AgBiBr_6$ have been successfully demonstrated, using both solid state reaction or solution processing methods.[22,23,24]. $Cs_2AgBiCl_6$ and $Cs_2AgBiBr_6$ appear as potential good candidates for solar absorbers in PSC.[22,23,] Despite the large band gap and indirect absorption, these materials exhibit extraordinarily long radiative emission lifetime of hundreds of ns, high defect tolerance, and higher stability of heat and moisture compared to conventional perovskites.[25] In addition, charge carrier effective masses of 0.14 m_e, close to those calculated for methylammonium lead iodide ($CH_3NH_3PbI_3$), have been derived.[24] All properties make this class of materials an interesting alternative for non-toxic PSCs. For $Cs_2AgBiBr_6$ single crystal and thin film, theoretical prediction and experimental work revealed band gaps of 1.83 eV[23] and 2.19 eV[22], respectively. However, their incorporation in PSC as active layer has so far been very limited, mainly due to the challenge in the preparation of high quality and compact double perovskite thin films. Although $Cs_2AgBiBr_6$ perovskite meso-structure solar cells has been shown by Greul et al.[26] with a PCE close to 2.4%, this value was extracted from a device characteristic severely affected by a huge hysteresis and *s*-shape, which casts some doubt on the real device performance. In addition, they adopted a fast crystallization process which impedes the formation of a smooth and homogeneous $Cs_2AgBiBr_6$ layer. Micrometer-large grains and a thick agglomerated morphology are formed on the capping layer, far from being the ideal morphology for a clean interface with the HTM in the sandwiched PSC. In our work, we adopted a different strategy for the optimization of a facile and highly reproducible deposition protocol to obtain a 200 nm thick homogeneous $Cs_2AgBiBr_6$ capping layer in the meso-structure solar cell architecture. Furthermore, we screened different

HTMs beyond the most used spiro-OMeTAD, to optimize the perovskite/HTM interface and device parameters. As a result, we fabricated lead-free PSCs with no hysteresis in the device characteristic, leading to a real PCE beyond 1% with high FF up to 0.7. This work establishes a defined and robust protocol and sets the basic guidelines for an optimized growth of $Cs_2AgBiBr_6$ perovskite active layers, resulting in a device behavior free from hysteresis artefacts. We believe that our approach will enable to surpass the current limits in the lead-free double perovskite technology, opening the way for a near-future massive device optimization.

Double perovskite materials are known to crystallize in the elpasolite structure, a highly symmetric face-centered cubic double-perovskite structure which can read as $A_2M^+M'^{3+}X_6$.[27] This structure consists of a network of corner-sharing octahedra, with Cs (for A) in the middle of the cuboctahedral cavity while the centers of the octahedra are either occupied by Bi or Ag (for M and M′, respectively) with alternating in a rock-salt configuration, as shown in Figure 1a. The $Cs_2AgBiBr_6$ film has been deposited by using spin coating deposition of solution 0.5M $Cs_2AgBiBr_6$ in dimethyl sulfoxide (DMSO) and annealing at high temperature. In more details, we first monitored the film growth and crystal quality varying the annealing temperatures in the range of 250 °C and 280 °C for 5 minutes. Figure 1b reports the X-ray diffraction pattern (XRD) of the double perovskite $Cs_2AgBiBr_6$ deposited on mesoporous TiO_2 (m-TiO_2)/FTO substrate. A main peak at 31.8° is present, representative of the (400) reflection of the double perovskite $Cs_2AgBiBr_6$, along with other main reflections (111, 200, 220, 311, 222, and 331). This pattern is evident for all the temperature range used, providing a solid proof for the successful formation of a phase-pure- double perovskite at temperature higher than 250 °C (see Supporting information Figure S1 for more details). Notably, no additional peak related to possible residuals of $Cs_3Bi_2Br_9$ or AgBr have been observed. In addition to the high temperature, we also introduced few other control

parameters to drive the material crystallization, aiming to obtain a homogeneous film with high crystal quality.[28] In particular, we adopted a second step in the deposition, known in the standard perovskite as an anti-solvent dropping technique. In this case, we dropped chlorobenzene during the film formation before the annealing step, aiming to obtain a compact and homogeneous layer without any pinholes. Overall, our optimization protocols enable the realization of a 200 nm thick $Cs_2AgBiBr_6$ film which shows a smooth and compact double perovskite layer with an average grain size of around 80 nm, as shown from the top surface of the scanning electron microscope (SEM) image in Figure 1d. This achievement represents a step forward in the optimization of the double perovskite morphology, which have highly challenged the community in the last year, especially relevant if compared to the state of the art showing a dishomogenous and disconnected island-like morphology. [26] As the $Cs_2AgBiBr_6$ film were optimized for photovoltaics, sufficiently thick material is mandatory for efficiently harvest the light. In order to optimize the optical absorption, i.e. the thickness of the film, we aimed at improving the infiltration of the double perovskite solution in the mesoporous oxide nanoparticle scaffold, by modifying the m-TiO_2 surface. More in details, we pre-treated the surface by UV-ozone for 15 min and by an additional $TiCl_4$ treatment. This lead to a change in the surface properties of m-TiO_2 overall further improving the material infiltration and crystallization, as shown by the SEM cross section image in Figure 1d. Improving the material morphology is an essential step to reduce pinholes and paths for charge recombination.[29] Overall, in our case the optimal combination of the mentioned modifications and adjustments, such as UV-ozone and $TiCl_4$ treatment[30] on TiO_2, preheating solution at 75°C before coating, anti-solvent dripping technique on spinning double perovskite layer,[31] along with the annealing at high temperatures, enabled the realization for the first time of a compact film of $Cs_2AgBiBr_6$. Notably, the choice of the solvent used also impact on the results obtained, indeed,

the use of different concentration of DMF and DMSO can results in a dishomogenous morphology (see Supporting information Figure S1c) and f)). The inclusion of the pre-heating step turned to be also of fundamental relevance for thin film optimization (Supporting information Figure S1). Figure 2 reports on the optical characterization of the $Cs_2AgBiBr_6$ thin film in terms of optical absorption and emission properties. Absorption spectra is reported in Figure 2a). From the Tauc plot a step profile is observed, with a first onset at around 2.4eV.[23] In the inset, the Tauc plot considering a direct band gap transition is also shown, giving a value for band gap of 2.20 eV, similarly to what already observed for $Cs_2AgBiBr_6$ thin films.[23] The retrieved band gap value is consistent with what reported in literature, within a variation range due to the different deposition approach used.[23] It is fair mentioning that, according to the Shockley–Queisser limit, a theoretical maximum PCE of 16.4% can be targeted with a material having a Eg of 2.2 eV, thus showing huge potential for working double perovskite based solar cells.[26] The $Cs_2AgBiBr_6$ emission results weak, as a consequence of the indirect band gap nature of the material. PL spectrum is reported in Fig 2b), peaking at 2.1eV. To assess the fate of photogenerated carriers measured the time-resolved PL decay, shown in Figure 2c, monitored at the emission peak. The PL intensity shows a fast initial drop (fitted with τ_1 = 5ns), followed by a slower one (τ_2 = 282ns), similarly to what observed for double perovskite thin films.[23] Notably, while the fast decay is associated to trap and/or surface-state emission, which, given the weak PL signal, in this case dominates. On the other side, the longer-lifetime processes may originate from fundamental charge recombination, in agreements with the long carrier lifetime extracted in $Cs_2AgBiBr_6$ single crystals, much longer, in this case with respect to standard methylammonium lead iodide based perovskites.[23]

We fabricated solar devices where the perovskite is sandwiched between the 2,2′,7,7′-tetrakis(N,N-dipmethoxyphenylamine)-9,9′-spirobifluorene (spiro-OMeTAD) hole-transporting

material and the mesoscopic TiO_2 scaffold (m-TiO_2) electron transporter in a standard mesoporous architecture. As known from literature[26] and represented in Figure 3a, the energy level diagram in shows that the conduction band (CB) of the $Cs_2AgBiBr_6$ is well aligned with the CB of the electron transporting mesoporous TiO_2. Aiming to improve the device performances we explored a series of different molecular and polymeric HTM having slightly different HOMO-LUMO values, as an energy diagram shown in Figure 3a. In addition to spiro-OMeTAD, typically used for lead perovskite solar cells, we considered the PTAA (Poly[bis(4-phenyl)(2,4,6-trimethylphenyl)amine]) and the PCPDTBT (Poly[2,1,3-benzothiadiazole-4,7-diyl[4,4-bis(2-ethylhexyl)-4H-cyclopenta[2,1-b:3,4-b']dithiophene-2,6-diyl]]), used in PSCs literature as polymeric HTMs.[32,33]

The current−voltage (J−V) characteristics of the solar cells under simulated air mass 1.5 global standard sunlight (AM1.5G) are reported in Figure 3b and the device parameters summarized in Table 1. The best solar cell performances resulted from using PTAA as HTM. Short circuit current (J_{SC}) of 1.84 mA/cm^2 and open circuit voltage (V_{OC}) of 1.02 V are obtained, see Table 1. The spiro-OMeTAD based solar cells shows reasonable J_{SC}, and V_{OC} of around 0.64V (0.8V in the best case, see device data and statistics in Tables S1, S2). It is interesting to notice the high V_{OC} value obtained despite the similarities in the HOMO level between spiro-OMeTAD, PCPDTBT and PTAA, actually a little higher for the latest.[34] It is fair to mention that despite the interface energy level alignment represents a useful rule of thumbs for screening the best HTM and evaluating the device Voc, a direct link between HTM energy levels and device V_{OC} cannot be univocally derived. This is because device Voc can be affected by multiple parameters which simultaneously come into play. Interfacial energy level mismatch, any possible internal electric field established by the difference in the work functions of the interfacial layers, interface charge accumulation, bulk

charge recombination can all affect, parameters which are highly sensitive to the perovskite crystal quality and film morphology. [35, 36] We do not aim to address all the possible parameters and processes affecting the V_{OC}, which would extend beyond the scope of our work. However, we could notice that the optimization process of perovskite films itself, modifying the perovskite crystal quality, grain boundaries and film homogeneity, strongly influences the V_{OC} (see Figure S1 and S2). For instance, as shown in Figure S5, when we prepared a device using the perovskite film without the anti-solvent dropping step but keeping PTAA as HTM, we see a remarkable drop in the device V_{OC}, despite the same interfacial energy level alignment and device architecture.

The incident photon to current conversion efficiency (IPCE) spectrum (Supporting information Figure S4) shows a band edge at $\sim$ 525 nm which is in agreement with absorption edge in Figure 2a. On the other side, PCPDTBT based solar cells show reduced voltage as well as reduced photocurrent. This can come from the lower band gap of PCPDTBT, and lower LUMO level, which can decrease the charge transfer selectivity. Overall, this suggests that not only the interface energetics, but also the interface quality and photoinduced processes, such as charge recombination, are utmost to optimize the device performances. Device results are confirmed on a statistics of around 40 devices, as shown in the Supporting Information, Figure S3. An important characteristic that must be evaluated when measuring perovskite solar cells is the shape of the J-V curve measured at different scanning voltage direction. Indeed, for lead based perovskite, as well as for previously reported $Cs_2AgBiBr_6$ based solar cells[26] a significant difference has been observed, indicative of a hysteresis behavior. Despite the exact reasons behind that is still subject of ongoing debate, it is general consensus that effects such as light induced ion movement, "photo-instability", or structural deformations can overall contribute to the anomalous hysteresis behavior.[37,38,39,40] Even for $Cs_2AgBiBr_6$, this has been previously assigned to ion and defect

9

movement in the device, despite the totally different material structure and composition.[26] Figure 4 shows the J-V hysteresis for our devices using PTAA as HTM. Notably, our device shows a hysteresis free behavior, reporting nearly identical values for the device parameters extracted in back and forward configurations. This contrasts to what reported in literature so far by Greul et al. reporting a tremendous hysteresis due to migration of the halide anions and trapping/de-trapping of charge carriers.[26] We observe a different behavior: in our case, as shown in Figure 4, no difference in carrier collection during the forward and reverse scan is observed, leading, for the first time, to the observation of a hysteresis free device behavior in lead-free double perovskite solar cells. We ascribe this to an ideal, and compact film structure and morphology we obtained, which can reduce the material structural stability. Further work is ongoing to clarify this point to gain a deeper insights on the ion movement and interface charge accumulation dynamics.

In conclusion, we report for the first time the investigation on interface of lead-free double perovskite $Cs_2AgBiBr_6$ using a new deposition approach following a multi-step optimization protocol. This enabled the realization of compact thin film of $Cs_2AgBiBr_6$ double perovskite with an optimal infiltration into the m-TiO_2 oxide scaffold. When embodied in solar cells, different contact polymers as HTM have been considered. PTAA has been here adopted reaching maximal power conversion efficiency up to 1.26% and showing for the first time no device hysteresis. We believe that our method describes a robust and easy optimization approach of double perovskite thin films, paramount for hysteresis free lead free based solar cells. This will pave the way for further material and device investigations, providing clear direction for the massive exploration of lead-free perovskites solar cells, a viable alternative for non-toxic perovskite near-future commercialization.

Supporting Information

The supporting Information is available free of charge on the ACS Publications website at DOI:

XXXX

Additional data and figures and a detailed description of the experimental methods used are reported.

AUTHOR INFORMATION

[1] Group for Molecular Engineering of Functional Materials, Institute of Chemical Sciences and Engineering, Ecole Polytechnique Fédérale de Lausanne, Sion CH-1951, Switzerland.

[2] Institute for Materials Science and Center for Nanointegration Duisburg-Essen (CENIDE), University of Duisburg-Essen, Universitätsstraße 15, 45141 Essen

Corresponding Author

*Giulia.grancini@epfl.ch; doru.lupascu@uni-due.de; mdkhaja.nazeeruddin@epfl.ch

Notes

The authors declare no competing financial interest.

References

(1)   Yang, W. S.; Park, B. W.; Jung, E. H.; Jeon, N. J.; Kim, Y. C.; Lee, D. U.; Shin, S.S.; Seo, J.; Kim, E. K.; Noh, J. H.; et al. Iodide Management in Formamidinium-Lead-Halide–Based Perovskite Layers for Efficient Solar Cells, *Science*, **2017**, *356*, 1376–1379.

(2)   Correa-Baena, J. P.; Saliba, M.; Buonassisi, T.; Grätzel, M.; Abate, A.; Tress, W.; Hagfeldt, A. Promises and Challenges of Perovskite Solar Cells, *Science*, **2017**, *358*, 739–744.

(3)   Yang, Y. You, J. Make Perovskite Solar Cells Stable, *Nature*, **2017**, *544*, 155–156.

(4)   Berhe, T. A.; Su, W.-N.; Chen, C.-H.; Pan, C.-J.; Cheng, J.-H.; Chen, H.-M.; Tsai, M.-C.; Chen, L.-Y.; Dubale, A. A.; Hwang, B.-J. Organometal Halide Perovskite Solar Cells, *Energy Environ. Sci.*, **2016**, *9*, 323–356.

(5)   Eperon, G. E.; Habisreutinger, S. N.; Leijtens, T.; Bruijnaers, B. J.; van Franeker, J. J.; de Quilettes, D. W.; Pathak, S.; Sutton, R. J.; Grancini, G.; Ginger, D. S.; et al. The Importance of Moisture in Hybrid Lead Halide Perovskite Thin Film Fabrication, *ACS Nano*, **2015**, *9*, 9380–9393.

(6)   Wang, D.; Wright, M.; Elumalai, N. K.; Uddin, A. Stability of Perovskite Solar Cells, *Sol. Energy Mater Sol. Cells*, **2016**, *147*, 255–275.

(7)   Abate, A. Perovskite Solar Cells Go Lead Free, *Joule*, **2017**, *1*, 659–664.

(8)   Babayigit, A.; Duy Thanh, D.; Ethirajan, A.; Manca, J.; Muller, M.; Boyen, H.-G.; Conings, B. Assessing the Toxicity of Pb- and Sn-based Perovskite Solar Cells in Model Organism Danio Rerio, *Sci. Rep.*, **2016**, *6*, 18721.

(9)   Li, L.; Zhang, F.; Hao, Y.; Sun, Q.; Li, Z.; Wang, H.; Cui, Y.; Zhu, F. High Efficiency Planar Sn–Pb Binary Perovskite Solar Cells, *J. Mater. Chem. C*, **2017**, *5*, 2360–2367.

(10) Jiang, Y.; Zhang, H.; Qiu, X.; Cao, B. The Air and Thermal Stabilities of Lead-Free Perovskite Variant Cs_2SnI_6 Powder, *Mater. Lett.*, **2017**, *199*, 50–52.

(11) Qiu, X.; Cao, B.; Yuan, S.; Chen, X.; Qiu, Z.; Jiang, Y.; Ye, Q.; Wang, H.; Zeng, H.; Liu, J.; et al. From Unstable $CsSnI_3$ to Air-Stable Cs_2SnI_6, *Sol. Energy Mater Sol. Cells*, **2017**, *159*, 227–234.

(12) Giustino, F.; Snaith, H. J. Toward Lead-Free Perovskite Solar Cells, *ACS Energy Lett.*, **2016**, *1*, 1233–1240.

(13) Angelis, F.; deKamat, P. V. Riding the New Wave of Perovskites, *ACS Energy Lett.*, **2017**, *2*, 922–923.

(14) Angelis, F. de. Modeling Materials and Processes in Hybrid/Organic Photovoltaics, *Acc. Chem. Res.*, **2014**, *47*, 3349–3360.

(15) Liao, Y.; Liu, H.; Zhou, W.; Yang, D.; Shang, Y.; Shi, Z.; Li, B.; Jiang, X.; Zhang, L.; Quan, L. N.; et al. Highly Oriented Low-Dimensional Tin Halide Perovskites with Enhanced Stability and Photovoltaic Performance, *J. Am. Chem. Soc.*, **2017**, *139*, 6693–6699.

(16) Cao, D. H.; Stoumpos, C. C.; Yokoyama, T.; Logsdon, J. L.; Song, T.-B.; Farha, O. K.; Wasielewski, M. R.; Hupp, J. T.; Kanatzidis, M. G. Thin Films and Solar Cells Based on Semiconducting Two-Dimensional Ruddlesden–Popper $(CH_3(CH_2)_3NH_3)_2(CH_3NH_3)_{n-1}Sn_nI_{3n+1}$ Perovskites, *ACS Energy Lett.*, **2017**, *2*, 982–990.

(17) Lester R. Morss; M. Siegal; L. Stengerand Norman Edelstein. Preparation of Cubic Chloro Complex Compounds of Trivalent Metals: Cs_2NaMCl_6, *Inorg. Chem.*, **1970**, *9*, 1771–1775.

(18) Smit, W. M. A.; Dirksen, G. J.Stufkens, D. J. Infrared And Raman Spectra Of The Elpasolites Cs, NaSbCl, And Cs, NaBiCl, Evidence For A Pseudo Jahn-Teller Distorted Ground State, *J. Phys. Chem. Solids*, **1990**, *51*, 189–196.

(19) Urland, W. The Assessment of The Crystal Field Parameters For Fn-Electron Systems By The Angular Overlap Model. Rare-Earth Ions M^{3+} In Cs_2NaMCl_6, *Chem. Phys. Lett.*, **1981**, *83 (1)*, 116–119.

(20) Barbier, P.; Drache, M.; Mairesse, G.; Ravez. Phase Transitions in a $Cs_{2-x}K_{1+x}BiCl_6$ Solid Solutions, *J. Solid State Chem.*, **1982**, *42*, 130–135.

(21) Benachenhou, F.; Mairesse, G.; Nowogrocki, G.; Thomas, D. Structural Studies of Cs-K-Bi Mixed Chlorides Relation to the Crystal Structures of A_2BMX_6, A_3MX_6, and A_2MX_6, *J. Solid State Chem.*, **1986**, *65*, 13–26.

(22) McClure, E. T.; Ball, M. R.; Windl, W. Woodward, P. M. Cs_2AgBiX_6 (X = Br, Cl), *Chem. Mater.*, **2016**, *28*, 1348–1354.

(23) Slavney, A. H.; Hu, T.; Lindenberg, A. M.; Karunadasa, H. I. A Bismuth-Halide Double Perovskite with Long Carrier Recombination Lifetime for Photovoltaic Applications, *J. Am. Chem. Soc.*, **2016**, *138*, 2138–2141.

(24) Volonakis, G.; Filip, M. R.; Haghighirad, A. A.; Sakai, N.; Wenger, B.; Snaith, H. J.Giustino, F. Lead-Free Halide Double Perovskites via Heterovalent Substitution of Noble Metals, *J. Phys. Chem. Lett.*, **2016**, *7*, 1254–1259.

(25) Slavney, A. H.; Hu, T.; Lindenberg, A. M.; Karunadasa, H. I. A Bismuth-Halide Double Perovskite with Long Carrier Recombination Lifetime for Photovoltaic Applications, *J. Am. Chem. Soc.*, **2016**, *138*, 2138–2141.

(26) Greul, E.; Petrus, M. L.; Binek, A.; Docampo, P.; Bein, T. Highly Stable, Phase Pure $Cs_2AgBiBr_6$ Double Perovskite Thin Films for Optoelectronic Applications, *J. Mater. Chem. A*, **2017**, *5*, 19972–19981.

(27) Zhao, X.-G.; Yang, J.-H.; Fu, Y.; Yang, D.; Xu, Q.; Yu, L.; Wei, S.-H. Zhang, L. Design of Lead-Free Inorganic Halide Perovskites for Solar Cells via Cation-Transmutation, *J. Am. Chem. Soc.*, **2017**, *139*, 2630–2638.

(28) Cho, K. T.; Grancini, G.; Lee, Y.; Oveisi, E.; Ryu, J.; Almora, O.; Tschumi, M.; Schouwink, P. A.; Seo, G.; Heo, S.; et al. Selective Growth of Layered Perovskites for Stable and Efficient Photovoltaics, *Energy Environ. Sci.*, **2018**, *11*, 952–959.

(29) Ostapchenko, V. Effect of $TiCl_4$ Treatment on Different TiO_2 Blocking Layer Deposition Methods, *Int. J. Electrochem. Sci.*, **2017**, 2262–2271.

(30) Singh, T.; Miyasaka, T. Stabilizing the Efficiency Beyond 20% with a Mixed Cation Perovskite Solar Cell Fabricated in Ambient Air under Controlled Humidity, *Adv. Energy Mater.*, **2018**, *8*, 1700677.

(31) Konstantakou, M.; Perganti, D.; Falaras, P.; Stergiopoulos, T. Anti-Solvent Crystallization Strategies for Highly Efficient Perovskite Solar Cells, *Crystals*, **2017**, *7*, 291.

(32) Heo, J. H.; Im, S. H.; Noh, J. H.; Mandal, T. N.; Lim, C.-S.; Chang, J. A.; Lee, Y. H.; Kim, H.-j.; Sarkar, A.; Nazeeruddin, M. K.; et al. Efficient Inorganic–Organic Hybrid Heterojunction

Solar Cells Containing Perovskite Compound and Polymeric Hole Conductors, *Nat. Photonics*, **2013**, *7*, 486–491.

(33) Calió, L.; Kazim, S.; Grätzel, M.; Ahmad, S. Hole-Transport Materials for Perovskite Solar Cells, *Angew. Chem. Int. Ed. Engl.*, **2016**, *55*, 14522–14545.

(34) Jiménez-López, J.; Cambarau, W.; Cabau, L.; Palomares, E. Charge Injection, Carriers Recombination and HOMO Energy Level Relationship in Perovskite Solar Cells, *Sci. Rep.*, **2017**, *7*, 6101.

(35) Tang, Z.; Wang, J.; Melianas, A.; Wu, Y.; Kroon, R.; Li, W.; Ma, W.; Andersson, M. R.; Ma, Z.; Cai, W. et al. Relating Open-Circuit Voltage Losses to the Active Layer Morphology and Contact Selectivity in Organic Solar Cells, *J. Mater. Chem. A*, **2018**, *270*, 1789.

(36) Ravishankar, S.; Gharibzadeh, S.; Roldán-Carmona, C.; Grancini, G.; Lee, Y.; Ralaiarisoa, M.; Asiri, A. M.; Koch, N.; Bisquert, J.; Nazeeruddin, M. K. Influence of Charge Transport Layers on Open-Circuit Voltage and Hysteresis in Perovskite Solar Cells, *Joule*, **2018**, *2*, 788-798.

(37) Frost, J. M.; Walsh, A. What Is Moving in Hybrid Halide Perovskite Solar Cells? *Acc. Chem. Res.*, **2016**, *49*, 528–535.

(38) Bi, E.; Chen, H.; Xie, F.; Wu, Y.; Chen, W.; Su, Y.; Islam, A.; Grätzel, M.; Yang, X.; Han, L. Diffusion Engineering of Ions and Charge Carriers for Stable Efficient Perovskite Solar Cells, *Nat. Commun.*, **2017**, *8*, 15330.

(39) Kim, H.-S.; Jang, I.-H.; Ahn, N.; Choi, M.; Guerrero, A.; Bisquert, J.; Park, N.-G. Control of I-V Hysteresis in $CH_3NH_3PbI_3$ Perovskite Solar Cell, *J. Phys. Chem. Lett.*, **2015**, *6*, 4633–4639.

(40) Bastiani, M. de; Dell'Erba, G.; Gandini, M.; D'Innocenzo, V.; Neutzner, S.; Kandada, A. R. S.; Grancini, G.; Binda, M.; Prato, M.; Ball, J. M.; et al. Ion Migration and the Role of Preconditioning Cycles in the Stabilization of the J-V Characteristics of Inverted Hybrid Perovskite Solar Cells, *Adv. Energy Mater.*, **2016**, *6*, 1501453.
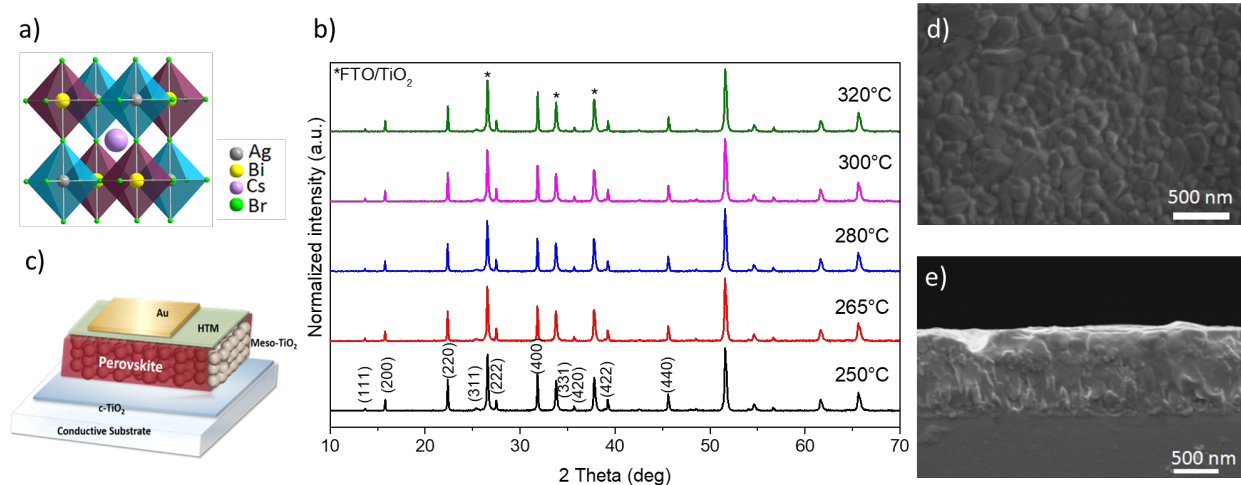
Figures and Table:

Figure 1. a) Cartoon of the Crystal structure of lead-free $Cs_2AgBiBr_6$ double perovskite. b) X-Ray diffraction (XRD) pattern of $Cs_2AgBiBr_6$ thin films deposited on mesoporous TiO_2 substrate at different annealing temperatures as indicated in the legend. c) Sketch of the device architecture used consisting of the double perovskite infiltrated in the mesoporous TiO_2 substrate and sandwiched, on top, with an organic HTM and gold top electrode. d) Scanning Electron Microscope (SEM) top view of the double perovskite layer obtained upon spin coating at room temperature using the anti-solvent treatment with chlorobenzene, e) SEM cross-section of the

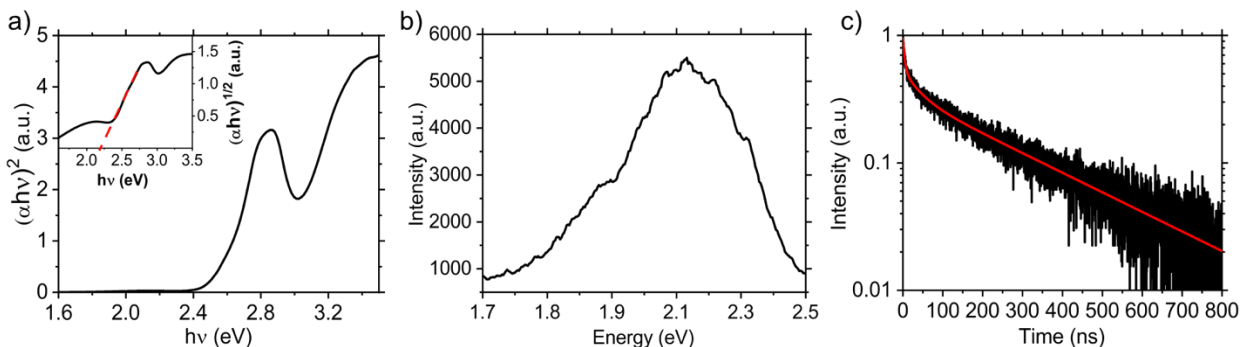FTO/c-TiO$_2$/m-TiO$_2$/double perovskite sample, upon annealing at 280 °C. Scalebar shown in the figure.

Figure 2. a) Absorption spectrum plotted in the form of Tauc plot, for an indirect bandgap, of the Cs$_2$AgBiBr$_6$ thin film deposited on glass (black). In inset, the Tauc plot for a direct bandgap with the dashed red line representing the linear fit for the band edge estimation. b) Photoluminescence (PL) spectra of the Cs$_2$AgBiBr$_6$ thin film. c) PL decay monitored at 2.1 eV. The decay is fitted using a bi-exponential function, resulting in fitted time constants of τ_1 = 5ns and τ_2= 282ns (red).

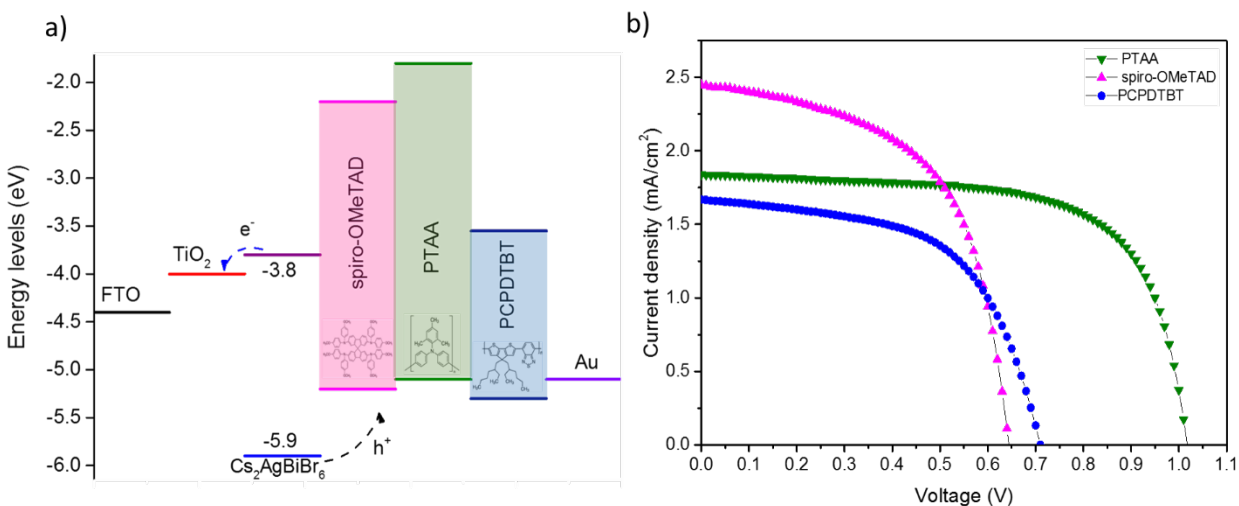**Figure 3.** a) scheme of corresponding energy level diagram with the following energy values; FTO (-4.4eV), TiO$_2$(-4.0eV), Cs$_2$AgBiBr$_6$ (HOMO; -5.9eV and LUMO; -3.8eV), spiro-OMeTAD (-

5.2eV, -2.2eV), PTAA (-5.1eV, -1.8eV), PCPDTBT (-5.3eV, -3.55eV) and Au (-5.1 eV), b) J-V

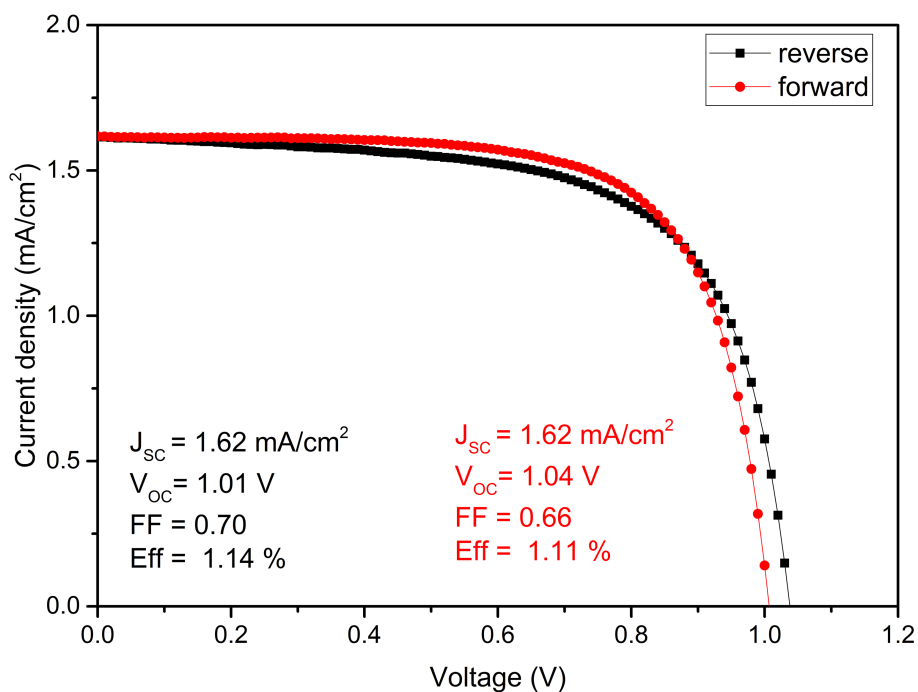curves for best performance solar cells using different HTMs

J-V curve plot: Current density (mA/cm²) vs Voltage (V), showing reverse (black) and forward (red) scans.

Black (reverse):
J_{SC} = 1.62 mA/cm^2
V_{OC}= 1.01 V
FF = 0.70
Eff = 1.14 %

Red (forward):
J_{SC} = 1.62 mA/cm^2
V_{OC}= 1.04 V
FF = 0.66
Eff = 1.11 %

Figure 4. Current – Voltage (J-V) curves of forward and reverse scan showing no hysteresis.

Device parameters are reported in the inset.

Table 1. Photovoltaic parameters of devices based on the different HTMs; Short –circuit current density (J_{SC}), Open-Circuit Voltage (V_{OC}), Fill Factor (FF) and Power Conversion Efficiency (PCE). Notably, device statistics has been conducted on 44 devices (spiro-OMeTAD), 27 devices (PTAA), 6 devices (PCPDTBT), see Supporting information for more details.

HTM	J_{SC} (mA/cm²)	V_{OC} (V)	FF	PCE (%)
PCPDTBT	1.67	0.71	0.57	0.68
spiro-OMeTAD	2.45	0.64	0.57	0.90
PTAA	1.84	1.02	0.67	1.26